Distributed and boundary control problems for the semidiscrete Cahn-Hilliard/Navier-Stokes system with nonsmooth Ginzburg-Landau energies

M. Hintermüller

Humboldt-Universität zu Berlin, Department of Mathematics, Germany

D. Wegner

Humboldt-Universität zu Berlin, Department of Mathematics, Germany

Abstract

This paper is concerned with optimal control problems for the coupled Cahn–Hilliard/Navier–Stokes system related to 'model H' of Hohenberg and Halperin [20]. It proposes a time-discretization allowing suitable energy estimates, that in particular force the total energy to decrease without control action, and it considers distributed as well as boundary control of the fluid. For non-smooth potentials, including the double-obstacle potential contained in the associated Ginzburg-Landau energy, a regularization procedure based on a mollified Moreau-Yosida approximation is applied. The resulting regularized problems are discretized by finite elements and solved via a gradient descent method. Several numerical examples document the behavior of the algorithm as well as the controlled Cahn–Hilliard/Navier–Stokes system for boundary and for distributed control.

1. Introduction

The renowned Cahn-Hilliard equation (CH) [9] is widely used for modeling phase separation and coarsening processes with a diffusive interface in multiphase systems. Whenever hydrodynamic effects are present, CH has to be coupled with an equation that describes the motion of the fluid.

The resulting coupled system is used to model polymer blends, proteins crystallization, cf. [23] and references within, or the solidification of liquid metal alloys [12]. It is utilized in the simulation of bubble dynamics (as in

nitrobenzene), in Taylor flows [1, 4] or for pinch-offs of liquid-liquid jets [22]. Moreover, it is applied to describe the effects of surfactants such as colloid particles at fluid-fluid interfaces in gels and emulsions used in food, pharmaceutical, cosmetic, or petroleum industries [2, 5, 26]. Even the simulation of cooling systems in nuclear power plants or applications in computer graphics are conducted by using these models [3].

In this paper we consider the following model related to 'model H' of Hohenberg and Halperin [20]:

$$\begin{aligned} \partial_t c - \tfrac{1}{Pe}\Delta w + \nabla c \cdot v &= 0, && (1.1)\\ -w - \varepsilon \Delta c + \Phi'(c) &\ni 0, && (1.2)\\ \partial_t v - \tfrac{1}{Re}\Delta v + (v\cdot\nabla)v - Kw\nabla c + \nabla \pi &= 0, && (1.3)\\ \operatorname{div} v &= 0, && (1.4) \end{aligned}$$

which models a two-phase flow subject to phase separation. The system (1.1)–(1.2) is the Cahn–Hilliard (CH) system, and (1.3)–(1.4) is the Navier–Stokes (NS) system for modeling fluid flow. Here, these equations are assumed to hold in a suitable spatial domain $\Omega \subset \mathbb{R}^N$ with $N \in \{1, 2, 3\}$ and for all times in a given time interval $(0, T)$ with $T > 0$. The quantity c is the concentration of the fluid phase with $c = 1$ or $c = -1$ describing the pure phases, respectively, and $c \in (-1, 1)$ an associated mixed state. Hence, c attains values within the interval $[-1, 1]$, only. The related chemical potential is given by w, the velocity of the fluid is denoted by v and the corresponding pressure by π. Moreover, the constant $\frac{1}{Pe}$ is the mobility coefficient of the system with Pe being the Péclet number, K measures the strength of the capillary forces, ε relates to the thickness of the interfacial region and Re is the Reynolds number. The terms $\nabla c \cdot v$ in (1.1) and $Kw\nabla c$ in (1.3) couple both systems.

The function Φ in (1.2) is the homogeneous free energy density in the Ginzburg-Landau energy model associated with the Cahn–Hilliard system. Whenever it is nonconvex, then a homogeneous mixture of the fluid is in general not a minimizer of the pertinent free energy functional. As a consequence phase separation can occur. Popular choices of Φ assume the decomposition of Φ into the smooth nonconvex part $-\frac{1}{2}c^2$ and a convex, but possibly nonsmooth part $\psi(c)$, i.e. $\Phi(c)(x) = \psi(c(x)) - \frac{1}{2}c^2(x)$. Within this family of potentials the double-well potential corresponding to $\psi(c) = c^4$ is smooth and admits the concentration c to attain values outside of the physically meaningful range $[-1, 1]$. While the differentiability properties of

the double-well potential yield mathematical convenience, the possibly unphysical range of c limits its ability to predict long time behavior of the phase separation process. On the other hand, the logarithmic potential $\psi(c) = (1+c)\ln(1+c) + (1-c)\ln(1-c)$ forces the concentration to take values inside $(-1, 1)$ only, rendering the pure phase $c = -1$ and $c = +1$ singular. This potential was already considered in Cahn's and Hilliard's original work [9] and it is used in the Flory-Huggins theory for modeling the phase separation in polymer solutions. Finally, the double-obstacle potential with $\psi(c) := 0$ if $|c| \leq 1$ and $\psi(c) := +\infty$ if $|c| > 1$ ensures the concentration to attain physically meaningful values only and it admits the pure phases $c = \pm 1$. This potential is also used in the context of polymer solutions and it appears appropriate in cases of deep quenches and rapid wall-hardening, cf. [25]. In contrast to the double-well and the logarithmic potential that possess differentiability properties and where $\psi'(c)$ (and thus $\partial\psi(c) = \{\psi'(c)\}$) is uniquely given, the derivative of the convex part ψ of the double-obstacle potential has to be understood in the sense of the (possibly set-valued) subdifferential $\partial\psi$ for convex functions. Hence, in a pure phase, i.e. either $c = 1$ or $c = -1$, $\partial\psi$ is both multi-valued and unbounded, which clearly complicates the analytic as well as the numerical treatment of the system (1.1)–(1.4).

In many applications one is interested in influencing the phase separation process. For instance, in binary alloys one typically tries to avoid or reduce separation effects since they drastically reduce the durability and the lifetime of the alloy. In the formation of polymeric membranes by an immersion precipitation process, where a polymer solution is immersed into a coagulation bath containing a nonsolvent, the decomposition of the polymeric solution has to be controlled in such a way that the final polymer has a given porosity pattern. The resulting morphological structure significantly influences the properties of the polymer membrane [33].

In this paper we therefore consider an optimal control problem for the coupled Cahn-Hilliard/Navier-Stokes system where the control u acts either as a distributed force entering (1.3) as a right hand side or as a boundary control for the fluid velocity. While boundary control of the fluid can be realized by various devices, e.g. blowing and suction, a typical distributed control would rely on electro-magnetic fluids. For reasons of well-posedness we close the system by appropriate boundary conditions on c, w and v, and

initial conditions on c and v. Thus, we study the problem

$$\min \mathcal{J}(c, v, u) \text{ subject to the semidiscrete CH-NS system with control } u, \tag{P}$$

where $\mathcal{J}$ represents a suitably chosen optimization objective (cost function).

Note that in contrast to other forms of controlling this system like receding horizon or instantaneous control techniques [21, 10, 19], where optimization of the corresponding control actions is only considered within one time step or over a small time horizon, we consider an optimal control problem over the whole time interval. Hence, the entire semi-discrete version of CH-NS is taken as a constraint system in the minimization context leading to an optimal balance with respect to the cost function between control costs and e.g. closeness to a desired profile. Upon analyzing stationarity conditions for (P), the discretization process is completed by applying the finite element method in space.

We note that the derivation of stationarity conditions for (P) is a delicate matter. This is in particular true when Φ involves the nonsmooth double-obstacle potential. In fact, in the latter case, (1.2) is equivalent to a variational inequality which is known to represent a degenerate constraint [7, 17, 18] in (P). As a consequence, one cannot apply the Karush–Kuhn–Tucker theory [34] for deriving stationarity conditions. In order to overcome this difficulty, in [18] a technique utilizing a mollified Moreau–Yosida approximation of Ψ is applied. Upon passage to the limit with the involved smoothing parameters a so-called C-stationarity system is obtained. On the numerical level this proof technique requires the solution of a sequence of nonlinear programs in Banach space where the limit process with respect to the smoothing parameters is based on a path-following scheme. While [18] merely contains theoretical results for boundary control problems only, the present work extends the scope of [18] to distributed control problems and, in particular, it offers a discretization and gradient-based solution scheme along with a report on various test cases involving the double-obstacle potential.

Let us further mention that the literature on the optimal control of the coupled semidiscrete CH-NS system is, to the best of our knowledge, essentially void apart from the analytic result given in [18]. Instantaneous control of the semidiscrete CH-NS system has been considered in [19] and optimal control problems in one dimension for the viscous as well as for the convective Cahn-Hilliard equation has been studied in [31] and [32]. For the sole Cahn-Hilliard or the Allen-Cahn equation optimal control problems were studied

from an analytic perspective in [15, 29, 30, 17, 14].

The rest of this paper is organized as follows: In section 2 we present a semi-discrete version of (1.1)–(1.4) and related optimal control problems with boundary or distributed control, respectively. Moreover, corresponding first order optimality conditions are given for smooth potentials ψ. Section 3 presents a mollified Yosida approximation that we apply to the subdifferential of ψ in order to find a stationarity condition for the original optimal control problem with the double-obstacle potential upon passage to the limit with the smoothing parameters in the mollified Yosida approximation. The resulting, smooth auxiliary problems can be solved by a gradient descent method and a path-following scheme which yields C-stationary points for the optimal control problem in the limit. An outline of the algorithm and its numerical realization is presented is given. The utilized finite element spaces are introduced in section 4. Various examples showing the behavior of the algorithm for boundary as well as for distributed control are contained in section 5. Section 6 summarizes the present work and the appendix provides our expansion of the Armijo line search algorithm.

2. Optimal control problem for the time-discretization

For its numerical realization, we discretize the above system (1.1)–(1.4) in time by using a semi-implicit Euler scheme. For this purpose, we fix a final time $T > 0$, a number of time steps $M \in \mathbb{N}$ and the corresponding time step size $\tau := T/M$. The value of the concentration at time $t_i = i\tau,\ i \in \{0, ..., M\}$, is denoted by c_i and $c = (c_0, ..., c_M)$ is the vector of concentrations at the discrete times $t_i,\ i = 0, ..., M$. We proceed analogously with other time-dependent quantities.

The time-discrete Cahn-Hilliard/Navier-Stokes system is given by

$$\begin{aligned}
\frac{1}{\tau}(c_{i+1} - c_i) - \tfrac{1}{Pe}\Delta w_{i+1} + \nabla c_i \cdot v_{i+1} &= C_i^1 && \text{(in } \Omega\text{)}, && (2.1)\\
-w_{i+1} - \varepsilon\Delta c_{i+1} - c_i + \partial\psi(c_{i+1}) &\ni C_i^2 && \text{(in } \Omega\text{)}, && (2.2)\\
\frac{1}{\tau}(v_{i+1} - v_i) - \tfrac{1}{Re}\Delta v_{i+1} + (v_i \cdot \nabla)v_{i+1} & \\
-Kw_{i+1}\nabla c_i + \nabla\pi_i &= \eta^{(1)}u_i^{(1)}, && \text{(in } \Omega\text{)}, && (2.3)\\
\textstyle\int_\Omega c_i = 0, \quad \int_\Omega w_i = 0, \quad \operatorname{div} v_i &= 0 && \text{(in } \Omega\text{)}, && (2.4)\\
\nabla c_i \cdot \vec{n} = 0, \quad \nabla w_i \cdot \vec{n} = 0, \quad v_i &= \eta^{(2)}u_i^{(2)} && \text{(on } \partial\Omega\text{)}, && (2.5)\\
c_0 = c_a, \quad v_0 = v_a & && \text{(in } \Omega\text{)}. && (2.6)
\end{aligned}$$

Here, the convex part of the homogeneous free energy density is given by a proper, convex and lower-semicontinuous functional $\psi : \mathbb{R} \to \overline{\mathbb{R}}$, and $C^i = (C_0^i, ..., C_M^i) \in \mathbb{R}^{M+1}$ for $i \in \{1, 2\}$ denotes the tuple of constant functions on Ω with possibly different values on each time slice. The reason for using these constants is the following. By condition (2.4) we enforce c_i and w_i to have vanishing mean values, respectively. For w this provides no restriction and is used in order to obtain a unique w (note here that a shift $w_i \mapsto w_i + C$ does not change the dynamics of the system in the sense that $K(w_{i+1}+C)\nabla c_i + \nabla \pi_i = K w_{i+1} \nabla c_i + \nabla(\pi_i + C c_i)$ would only replace the pressure π_i by $\pi_i + C c_i$). For c, on the other hand, $\nabla c_i \cdot v_{i+1}$ can only be expected to have mean value 0 if $c_i v_{i+1}$ has no normal contribution on the boundary. Indeed, one has

$$\int_\Omega K \nabla c_i \cdot v_{i+1} = K \int_{\partial\Omega} c_i v_{i+1} \cdot \vec{n} - K \int_\Omega c_i \operatorname{div} v_{i+1} = K \int_{\partial\Omega} c_i v_{i+1} \cdot \vec{n}$$

for smooth c_i and v_{i+1}. While the mean-value property is problematic in the boundary control case, it is satisfied in the case of distributed control. For boundary control problems of the fluid we simplify our model by projecting the concentration onto the space of functions with zero mean value. Hence, we impose the conditions (2.4) and introduce in equation (2.1) the correction term C_i^1 which corresponds to the mean value of $\nabla c_i \cdot v_{i+1}$. As a consequence, we obtain $\int_\Omega c_{i+1} = 0$. In order to keep these corrections small, for boundary control we only use examples with one pure phase in a boundary layer as initial data. In this case, ∇c_i can be expected to be small, if not zero.

In this paper we consider either the case of Dirichlet boundary control (which corresponds to $\eta^{(1)} = 0$) or the case of distributed control acting as an additional force on the fluid entering the system as a right hand side in the balance of momentum (in this case set $\eta^{(2)} = 0$). Of course, also a combined control action consisting of both types of controls could be studied using the techniques discussed in the present paper.

For the concentration c and the chemical potential w, Neumann boundary conditions are imposed by (2.5). The conditions (2.4) forces both quantities to preserve a vanishing mean value and the velocity to be divergence-free. Note that in our examples below we normally assume initial values for the concentration which do not meet this mean value condition. Hence, we shift the whole problem via $\hat{c} := c - \overline{c}$ with $\overline{c} := \frac{1}{|\Omega|} \int_\Omega c$ and use $\hat{c}$ instead of c. The shifted concentration $\hat{c}$ satisfies the mean value condition in (2.4). As a consequence, the interval $[-1, 1]$ is shifted to $[-1 - \overline{c}, 1 - \overline{c}]$ and the potential ψ has to be adapted accordingly.

Apart from the additional right hand side in (2.3) corresponding to the distributed control, this setting was used in [18] in order to prove the existence of optimal boundary controls and to derive stationarity conditions.

We note that the above discretization scheme allows to derive energy estimates for the total energy of the system in each time step. In particular, in the case that no control action is applied, the total energy decreases monotonically. This was a key property in the proof of existence of optimal controls; see [18] for details. Also note that in discretization schemes, as for instance the one used in [16] where the Cahn-Hilliard and the Navier-Stokes part decouple from each other, such energy estimates cannot be expected to hold true.

Here we exemplarily study the following cost functional on $H^1(\Omega)\times U^{(1)}\times U^{(2)}$ given by

$$\mathcal{J}(c,u^{(1)},u^{(2)}) := \sum_{i=0}^{M} \lambda_i \|c_i - c_i^*\|_{L^2}^2 \;+\; \eta^{(1)}\|u_i^{(1)}\|_{L^2}^2 \;+\; \eta^{(2)}\|u_i^{(2)}\|_{H^{1/2}}^2 \quad (2.7)$$

for closed subspaces $U^{(1)}$ of $H^1_\sigma(\Omega) := \{v \in H^1(\Omega;\mathbb{R}^N) \mid \operatorname{div} v = 0\}$ and $U^{(2)}$ of $U := \{\operatorname{Tr} v \,|\, v \in H^1(\Omega;\mathbb{R}^N),\ \operatorname{div} v = 0\}$ which itself is a closed subspace of $H^{1/2}(\partial\Omega;\mathbb{R}^N)$. Here and below Tr denotes the trace-operator. We note that, of course, other objectives are conceivable. We equip the space $H^{1/2}(\partial\Omega;\mathbb{R}^N)$ with the norm $\|u\|_{H^{1/2}} := \{\inf ||v||_{H^1(\Omega;\mathbb{R}^N)} \mid v \in H^1(\Omega;\mathbb{R}^N),\ \operatorname{Tr} v = u\}$ and $H^1(\Omega;\mathbb{R}^N)$ with the standard norm $\|v\|_{H^1} := (\sum_{n=1}^N \|v^n\|_{H^1}^2)^{1/2}$ for $v = (v^1,...,v^N) \in H^1(\Omega;\mathbb{R}^N)$, $\|v\|_{H^1} := (\|v\|_{L^2}^2 + \| \,|\nabla v|\, \|_{L^2}^2)^{1/2}$ for $v \in H^1(\Omega)$ with the Euclidian norm $|\,.\,| : \mathbb{R}^N \to \mathbb{R}$. The corresponding optimal control problem (P_ψ) depending on the choice of the potential ψ is then given by

$$\begin{aligned}\min \big\{ \mathcal{J}(c,u^{(1)},u^{(2)}) \mid (c,w,v,u^{(1)},u^{(2)}) \in \\ \big(H^1(\Omega)\times H^1(\Omega)\times H^1(\Omega;\mathbb{R}^N)\times U^{(1)}\times U^{(2)}\big)^{M+1} \\ \text{satisfies (2.1)–(2.5) in the weak sense}\big\}.\end{aligned}$$

In particular we are interested in the case $\psi = \varphi^{(0)}$ of the double-obstacle potential, i.e.

$$\varphi^{(0)} : \mathbb{R} \to \overline{\mathbb{R}}, \quad \varphi^{(0)}(r) := \begin{cases} 0 & \text{if } |r| \le 1, \\ \infty & \text{otherwise.} \end{cases} \quad (2.8)$$

For (P_ψ) the existence of a minimizer together with first order optimality conditions respectively stationarity conditions were established in [18] in the

case of boundary control.
Using the arguments of [18] and proceeding in a similar way for the problem setting including distributed control, the gradient of the *reduced* cost functional $\hat{\mathcal{J}}(u^{(1)}, u^{(2)}) := \mathcal{J}(c(u^{(1)}, u^{(2)}), u^{(1)}, u^{(2)})$ for a solution (c, w, v, u) of (2.1)–(2.5) and for a smooth potential ψ can be written, with the help of J, the duality mapping of $[(U^{(1)} \times U^{(2)})]^{M+1}$, as

$$J^{-1}\hat{\mathcal{J}}'(u^{(1)}, u^{(2)}) = (\eta^{(1)}u^{(1)} - z^{(1)}, \eta^{(2)}u^{(2)} - z^{(2)})$$

with $(z^{(1)}, z^{(2)}) \in (U^{(1)} \times U^{(2)})^{M+1}$ given by $z_0^{(i)} = 0$ for $i = 1, 2$ and

$$\begin{aligned} -\frac{1}{\tau}(p_{i+1} - p_i) + (-\varepsilon\Delta + DA(c_{i+1}))^*(-\tfrac{1}{Pe}\Delta p_i - K\nabla c_i \cdot q_i) & \\ -(-\tfrac{1}{Pe}\Delta p_{i+1} - K\nabla c_{i+1} \cdot q_{i+1}) & \\ - \operatorname{div}(p_{i+1}v_{i+2}) + K \operatorname{div}(w_{i+2}q_{i+1}) &= C_i^3 + \lambda_i J_{W_0}(c_i - c_i^*), \quad (2.9) \\ -\frac{1}{\tau}(q_{i+1} - q_i) - \tfrac{1}{Re}\Delta^* q_i + b_1(v_{i+2}, q_{i+1}) + b_2(v_i, q_i) & \\ +p_i\nabla c_i &= -\nabla\pi_i^2, \quad (2.10) \\ \textstyle\int_\Omega p_i = 0, \quad \operatorname{div} q_i &= 0, \quad (2.11) \\ -J_{U^{(1)}}^{-1} I^*_{U^{(1)}\to V_{-1}} q_i &= z_{i+1}^{(1)}, \quad (2.12) \\ H\big[-\frac{1}{\tau}(q_{i+1} - q_i) - \tfrac{1}{Re}\Delta q_i + b_1(v_{i+2}, q_{i+1}) & \\ +b_2(v_i, q_i) + p_i\nabla c_i\big] &= z_{i+1}^{(2)}. \quad (2.13) \end{aligned}$$

Here, $A := \partial\psi$, $I_{U^{(1)}\to V_{-1}}$ is the canonical injection of $U^{(1)}$ into V_{-1} and $H : (H^1(\Omega; \mathbb{R}^N))^* \to U^{(2)}$ denotes the composition $H = P_{U^{(2)}} \circ \operatorname{Tr} \circ P_Z \circ J_{H^1}^{-1}$ consisting of the orthogonal projection $P_{U^{(2)}}$ of U onto $U^{(2)}$, the orthogonal projection P_Z of $H^1(\Omega; \mathbb{R}^N)$ onto $Z := \{z \in H^1(\Omega; \mathbb{R}^N) \,|\, \operatorname{div} z = 0, (z|v)_{H^1} = 0 \ \forall v \in H_0^1(\Omega; \mathbb{R}^N), \operatorname{div} v = 0\}$ and the inverse of J_{H^1}. Here, for a Hilbert space X, the operator J_X denotes the canonical isomorphism from X onto X^* given by the Riesz-representation theorem [27]. By $(\,.\,|\,.\,)_{H^1}$ we denote the inner product of $H^1(\Omega; \mathbb{R}^N)$, and b_1 and b_2 are related to the convective part of the NS equation by

$$\langle b_1(y_2, y_3), y_1\rangle := \langle b_2(y_1, y_3), y_2\rangle := \int_\Omega y_3(x)(y_1(x) \cdot \nabla)y_2(x)\, dx.$$

with $\langle .,. \rangle$ denoting the duality pairing between $H^1_\sigma(\Omega)^*$ and $H^1_\sigma(\Omega)$. For an operator S, S^* denotes its adjoint. Moreover, since (p,q) take values $((p_0,...,p_{M-1}),(q_0,...,q_{M-1}))$ we use the convention $(p_M,q_M)=0$ which was already used in the system (2.9)–(2.13). As a consequence of this convention, we do not have to denote the final time conditions on (p,q) explicitly. We further note that the notation of the reduced cost functional alluded to above corresponds to the situation where c (and w) is no longer considered an independent variable, but rather it is viewed as a function of $u^{(1)}$ and $u^{(2)}$, i.e., $c=c(u^{(1)},u^{(2)})$ where c and $u^{(1)},u^{(2)}$ are linked by solving (2.1)–(2.6).

It is possible to rewrite (2.9) in a fashion more similar to (2.1)–(2.2). In fact, we introduce another variable r which satisfies $\int_\Omega r=0$ as well as the system

$$\begin{aligned} -\frac{1}{\tau}(p_{i+1}-p_i)+(-\varepsilon\Delta+DA(c_{i+1}))^* r_i & \\ -I^*(-\tfrac{1}{Pe}\Delta p_{i+1}-K\nabla c_{i+1}\cdot q_{i+1}) & \\ -\operatorname{div}(p_{i+1}v_{i+2})+K\operatorname{div}(w_{i+2}q_{i+1}) &= C_i^3+\lambda_i J_{W_0}(c_i-c_i^*),\\ -r_i+(-\tfrac{1}{Pe}\Delta p_i-K\nabla c_i\cdot q_i) &= 0. \end{aligned}$$

3. Yosida approximation and gradient method

3.1. Sequential Yosida approximation

In order to derive first order optimality conditions for characterizing solutions of (P_ψ) in the case where $\psi=\varphi^{(0)}$, in [18] we replaced the potential $\varphi^{(0)}$ by a mollified Moreau-Yosida approximation. For this purpose, let $\rho\in C^1(\mathbb{R})$ denote a fixed mollifier with $\operatorname{supp}\rho\subset[-1,1]$, $\int_{\mathbb{R}}\rho=1$ and $0\le\rho\le 1$ almost everywhere (a.e.) on $\mathbb{R}$ and let $\epsilon:\mathbb{R}^+\to\mathbb{R}^+$ be a function with $\epsilon(\alpha)>0$ for $\alpha>0$ and $\frac{\epsilon(\alpha)}{\alpha}\to 0$ as $\alpha\to 0$. We consider the Yosida approximation β_α (with parameter $\alpha>0$) of $\beta:=\partial\varphi^{(0)}$ (for the general definition of the Yosida approximation we refer to [6]) and define

$$\rho(\epsilon)(s):=\frac{1}{\epsilon}\rho\Big(\frac{s}{\epsilon}\Big),\quad \widetilde{\beta}_\alpha:=\beta_\alpha*\rho_{\epsilon(\alpha)},\quad \gamma_\alpha(s):=\int_0^s\beta_\alpha,\quad \varphi_\alpha(c):=\int_\Omega\gamma_\alpha\circ c,$$

where '$*$' denotes the usual convolution operator and '$\circ$' represents composition. Here, $\widetilde{\beta}_\alpha$ is the mollification of the Yosida approximation β_α by a dilation of the convolution kernel ρ. Further, φ_α is a regularization of the potential $\varphi^{(0)}$ which is very similar to the Moreau-Yosida approximation but

it enjoys higher regularity. For $\alpha_n > 0$ we write $\varphi^{(n)} := \varphi_{\alpha_n}$ and $A^{(n)} := \partial\varphi^{(n)}$ for ease of notation.

Let $(\alpha_n)_{n\in\mathbb{N}},\ \alpha_n > 0$ for all $n \in \mathbb{N}$, denote a subsequence of reals with $\alpha_n \to 0$. In order to solve the optimization problem (P_ψ), we make use of the fact that a sequence of optimal controls for the problems $(\mathrm{P}_{\varphi^{(n)}})$ converges weakly in $(H^1(W_1) \times U^{(1)} \times U^{(2)})^{M+1}$ to a solution of (P_ψ) with even strong convergence in the first component; for a proof in the boundary control case we refer to [18, Theorem 3.6].

For the numerical solution of (P_ψ) we therefore fix such a sequence $(\alpha_n)_{n\in\mathbb{N}}$ and solve the sequence of problems $(\mathrm{P}_{\varphi^{(n)}})_{n\in\mathbb{N}}$. In the present work, each $(\mathrm{P}_{\varphi^{(n)}})$ is solved by a steepest descent method, which is initialized by an (approximate) stationary point of $(\mathrm{P}_\varphi^{(n-1)})$ for $n \geq 1$. The entire process is initialized by picking some $u^{(0)} \in (U^{(1)} \times U^{(2)})^{M+1}$.

3.2. Steepest descent method with expansive line search

Algorithmically, the steepest descent direction for the reduced objective $\hat{\mathcal{J}}(u)|_{u=u^{(n,k)}}$, where $u^{(n,k)},\ k \in \mathbb{N}$, denotes an actual approximation of $u^{(n)}$, a stationary point of $(\mathrm{P}_{\varphi^{(n)}})$, is computed as follows: Given $u^{(n,k)} \in (U^{(1)} \times U^{(2)})^{M+1}$ one solves the primal system (2.1)–(2.6), which yields $(c^{(n,k+1)}, w^{(n,k+1)}, v^{(n,k+1)})$. With this information at hand, the adjoint system (2.9)–(2.13) is solved yielding $(p^{(n,k+1)}, q^{(n,k+1)})$. Upon applying the Riesz-representation theorem [27], the gradient-based descent direction is given by

$$d^{(n,k)} = -J^{-1}\hat{\mathcal{J}}'(u^{(n,k)}) = (\eta^{(1)}u^{(1)} - z^{(1)}, \eta^{(2)}u^{(2)} - z^{(2)})$$

with $z^{(1)}$ and $z^{(2)}$ as given in (2.12) and (2.13) and with J denoting the duality mapping of $[(U^{(1)} \times U^{(2)})]^{M+1}$. In order to avoid the implementation of the $H^{1/2}(\Omega;\mathbb{R}^N)$-norm, we represent functions in U as their norm-minimal continuation into the space $H^1_\sigma(\Omega)$, which we equip with the norm induced by $H^1(\Omega;\mathbb{R}^N)$. Then the equations (2.12) and (2.13) for $z^{(1)}$ and $z^{(2)}$, respectively, involve the applications of $J^{-1}_{H^1}(\Omega;\mathbb{R}^N)$ for every $t_i,\ i = 1, ..., M$. Since the norm of $H^1(\Omega;\mathbb{R}^N)$ involves gradient terms, the computation of $J^{-1}_{H^1}(\Omega;\mathbb{R}^N)$ requires to solve a Dirichlet problem. In fact, for $u^{(2)} \in H^{1/2}(\Omega;\mathbb{R}^N)$ one needs to solve the following problem

$$\hat{u}^{(2)} = \operatorname{argmin}\{||u'||_{H^1(\Omega;\mathbb{R}^N)} \,:\, u' \in U^{(1)},\ \operatorname{Tr} u' = u^{(2)}\}.$$

Then, $\hat{u}^{(2)}$ represents the norm-minimal extension of $u^{(2)}$ to $H^1_\sigma(\Omega)$. The steepest descent direction $d^{(n,k)}$ is then used in an Armijo-type line search

with expansion (see Algorithm 1 in the appendix) in order to find a suitable step length $s^{(n,k)} > 0$ along $d^{(n,k)}$. The next control iterate is then given by

$$u^{(n,k+1)} := u^{(n,k)} + s^{(n,k)} d^{(n,k)}$$

and this process is repeated. We expand the standard Armijo line search (see e.g. [8]) in order to reduce the number of evaluations of the reduced objective since each evaluation corresponds to solving the entire primal system. For this purpose we initialize the line search parameter s by the value $s^{(n,k-1)}$ computed in the previous application of the line search algorithm. Then, the line search algorithm tests and, if necessary, replaces s by $w_c s$ for a constant factor $w_c < 1$ until the Armijo rule is fulfilled or s becomes smaller than the lower limit $s_{\min} > 0$. In the latter case the line search algorithm stops with a failure. In order to also allow increases of the step size, the algorithm checks whether the Armijo rule is satisfied for $w_e s$, with some fixed $w_e > 1$, in case the last z_z applications of the line search procedure terminated successfully with the respective initial step size. This expansion is applied for at most z_m consecutive steps.

We continue the gradient descent method as long as the decrease of the values of the objective is sufficiently large or there are still sufficient large changes in the primal variables. More precisely, if in a number z_s of consecutive gradient steps the new value $\mathcal{J}$ of the objective does not drop below $(1-\theta_n)\mathcal{J}_{\text{old}}$ with $\mathcal{J}_{\text{old}}$ denoting the value of the objective after the application of the previous descent step, and the changes $||c-c_{\text{old}}||_{L^2}$ and $||v-v_{\text{old}}||_{L^2}$ are smaller then $\vartheta_n||c_{\text{old}}||$ and $\vartheta_n||v_{\text{old}}||$, respectively, then we stop the gradient descent algorithm and proceed to the next Yosida parameter α_{n+1}. Here, $\vartheta_n, \theta_n > 0$ denote parameters which depend on n.

3.3. Newton's method for the primal system

The primal system is solved iteratively forward in time by using Newton's method. The latter converges at a local superlinear convergence rate. The adjoint system is linear and can be solved directly and iteratively backward in time. We note that the arguments given in [18] provide sufficient conditions for the existence of solutions to the respective system.

Next we exemplarily set-up the primal system as it is solved by Newton's method. Given $(c_i, w_i, v_i) \in H^1(\Omega) \times H^1(\Omega) \times H^1_\sigma(\Omega)$ at $t = t_i$, the tuple $(\widetilde{c}, \widetilde{w}, \widetilde{v}) = (c_{i+1}, w_{i+1}, v_{i+1})$ is computed such that

$$F(\widetilde{c}, \widetilde{w}, \widetilde{v}) = 0. \tag{3.1}$$

For all $(z_c, z_w, z_v) \in H^1(\Omega)\times H^1(\Omega)\times H^1_\sigma(\Omega)$ with $\int_\Omega z_c = \int_\Omega z_w = 0,\ \ z_v|_{\partial\Omega} = 0$ the variational form of (3.1) reads

$$\langle F(\widetilde{c},\widetilde{w},\widetilde{v}),(z_c,z_w,z_v)\rangle = \begin{pmatrix} (\widetilde{c} - c_i + \tau\nabla c_i\cdot\widetilde{v}\,|\,z_c) + \tau\frac{1}{Pe}(\nabla\widetilde{w}\,|\,\nabla z_c) \\ (-\widetilde{w} - c_i + \psi'(\widetilde{c})\,|\,z_w) + \varepsilon(\nabla\widetilde{c}\,|\,\nabla z_w) \\ (\widetilde{v} - v_i + (v_i\cdot\nabla)\widetilde{v} - K\widetilde{w}\nabla c_i)\,|\,z_v) + \frac{1}{Re}(\nabla\widetilde{v}\,|\,\nabla z_v) \end{pmatrix}$$

with $(f\,|\,g) := \int_\Omega fg$. Then, given some $(\widetilde{c}^{(0)},\widetilde{w}^{(0)},\widetilde{v}^{(0)}) \in H^1(\Omega)\times H^1(\Omega)\times H^1_\sigma(\Omega)$ and setting $l := 0$, the Newton iterations take the form

$$(\widetilde{c}^{(l+1)},\widetilde{w}^{(l+1)},\widetilde{v}^{(l+1)}) = (\widetilde{c}^{(l)},\widetilde{w}^{(l)},\widetilde{v}^{(l)}) + d^{(l)},$$

for d satisfying $\left\langle DF(\widetilde{c}^{(l)},\widetilde{w}^{(l)},\widetilde{v}^{(l)})d, z\right\rangle = -\left\langle F(\widetilde{c}^{(l)},\widetilde{w}^{(l)},\widetilde{v}^{(l)}), z\right\rangle$ for all $z = (z_c,z_w,z_v) \in H^1(\Omega)\times H^1(\Omega)\times H^1_\sigma(\Omega)$ with $\int_\Omega z_c = \int_\Omega z_w = 0,\ \ z_v|_{\partial\Omega} = 0$.

4. Finite element approximation

For the numerical realization of the aforementioned gradient descent procedure, the systems (2.1)–(2.6) and (2.9)–(2.13) are discretized in space. For this purpose let $\mathcal{T}$ denote a shape regular simplicial triangulation of Ω with $\overline{\Omega} = \bigcup_{T\in\mathcal{T}} T$. The corresponding set of faces of the elements in $\mathcal{T}$ is denoted by $\mathcal{E}$. We consider the following finite element spaces:

$$\begin{aligned} W^{\mathcal{T}} &:= \{w \in C^0(\overline{\Omega})\,|\,w|_T \in P_1(T) \quad \forall T\in\mathcal{T}\}, \\ V^{\mathcal{T}} &:= \{v \in L^\infty(\overline{\Omega})\,|\,v|_T \in P_1(T), \quad v|_{T_1}(E_m) = v|_{T_2}(E_m) \\ &\qquad\qquad \forall T,T_1,T_2\in\mathcal{T},\ \ E = T_1\cap T_2 \in \mathcal{E}\}, \end{aligned}$$

where E_m denotes the midpoint of a face $E\in\mathcal{E}$ and $P_1(T)$ is the space of affine functions on T. We use the space $W^{\mathcal{T}}$ of P_1-finite elements for the discretization of c, w and p and the LBB-stable Crouzeix-Raviart element space $V^{\mathcal{T}}$ (see [11]) for v and q.

The spatial discretization of (2.1)–(2.6) leads to finding $(c,w,v) \in (W^{\mathcal{T}}\times W^{\mathcal{T}}\times V^{\mathcal{T}})^{M+1}$ such that $\int_\Omega c = \int_\Omega w = 0,\ \ \operatorname{div} v = 0,\ \ v_{i+1}|_{\partial\Omega} = \eta^{(2)}u^{(2)}_{i+1},\ \ c_0 = c_a,\ \ v_0 = v_a$ and

$$\begin{aligned} (\frac{1}{\tau}(c_{i+1}-c_i) + \nabla c_i\cdot v_{i+1}\,|\,z_c) + \tfrac{1}{Pe}(\nabla w_{i+1}\,|\,\nabla z_c) &= 0, \\ (-w_{i+1} - c_i + \pi^{\mathcal{T}}\partial\psi(c_{i+1})\,|\,z_w) + \varepsilon(\nabla c_{i+1}\,|\,\nabla z_w) &= 0, \\ (\frac{1}{\tau}(v_{i+1}-v_i) + (v_i\cdot\nabla)v_{i+1} - Kw_{i+1}\nabla c_i\,|\,z_v) + \tfrac{1}{Re}(\nabla v_{i+1}\,|\,\nabla z_v) &= \eta^{(1)}(u^{(1)}\,|\,z_v) \end{aligned}$$

for all $(z_c, z_w, z_v) \in (W^{\mathcal{T}} \times W^{\mathcal{T}} \times V^{\mathcal{T}})^M$ with $\operatorname{div} z_v = 0$ and $\int_\Omega z_c = \int_\Omega z_w = 0$. Here, $\pi^{\mathcal{T}} : C(\overline{\Omega}) \to W^{\mathcal{T}}$ denotes the Lagrange interpolation operator [13]. Differential operators on vector fields in $V^{\mathcal{T}}$ are understood in the element-wise sense, i.e., $(\operatorname{div} v)|_T = \operatorname{div}(v|_T)$ a.e. and for all $T \in \mathcal{T}$, for instance. For the adjoint system we proceed similarly and use the spatially discretized version

$$\begin{aligned}
(-\frac{1}{\tau}(p_{i+1} - p_i) + K\nabla c_{i+1} \cdot q_{i+1} - \operatorname{div}(p_{i+1} v_{i+2}) & \\
+K \operatorname{div}(w_{i+2} q_{i+1}) \,|\, z_c) + (\varepsilon \nabla r_i - \tfrac{1}{Pe} \nabla p_{i+1} \,|\, \nabla z_p) & \\
+(r_i \,|\, DA(c_{i+1}) z_p) &= (\lambda_i (c_i - c_{ei}) \,|\, z_p), \\
(-r_i - K\nabla c_i \cdot q_i \,|\, z_r) + \tfrac{1}{Pe}(\nabla p_i \,|\, \nabla z_r) &= 0, \\
(-\frac{1}{\tau}(q_{i+1} - q_i) + b_1(v_{i+2}, q_{i+1}) + b_2(v_i, q_i) + p_i \nabla c_i \,|\, z_q) & \\
+\tfrac{1}{Re}(\nabla q_i \,|\, \nabla z_q) &= 0, \\
\int_\Omega p = 0, \quad \int_\Omega r = 0, \quad \operatorname{div} q &= 0, \\
-J^{-1}_{U^{(1)}} I^*_{U^{(1)} \to V_{-1}} q &= z_1, \\
H\big[-\frac{1}{\tau}(q_{i+1} - q_i) - \tfrac{1}{Re}\Delta q_i + b_1(v_{i+2}, q_{i+1}) & \\
+b_2(v_i, q_i) + p_i \nabla c_i \big] &= z_2.
\end{aligned}$$

We emphasis that the above discretization yields the exact gradient of the optimal control problem for the spatially discretized semidiscrete CH-NS system.

As mentioned above, we avoid the implementation of the $H^{1/2}(\Omega; \mathbb{R}^N)$ norm by representing functions in U as their norm-minimal continuation into the space $H^1_\sigma(\Omega)$, where the latter space is equipped with the induced norm of $H^1(\Omega; \mathbb{R}^N)$. This extension operator will be denoted by $\mathcal{F} : U \to H^1_\sigma(\Omega)$. Moreover, we reformulate (2.3) by replacing v by $\widetilde{v} + \mathcal{F}u$ and obtain

$$\begin{aligned}
&\frac{1}{\tau}(\widetilde{v}_{i+1} - \widetilde{v}_i) - \tfrac{1}{Re}\Delta \widetilde{v}_{i+1} + (\widetilde{v}_i + \mathcal{F}u_i \cdot \nabla)\widetilde{v}_{i+1} - K w_{i+1} \nabla c_i + \nabla \pi \\
&= \eta^{(1)} u^{(1)} - \Big[\mathcal{F}\frac{1}{\tau}(u_{i+1} - u_i) - \tfrac{1}{Re}\Delta u_{i+1} + (\widetilde{v}_i + \mathcal{F}u_i \cdot \nabla)\mathcal{F}u_{i+1} \Big], \qquad (4.1)
\end{aligned}$$

where $\widetilde{v}$ satisfies homogeneous Dirichlet boundary conditions.

In order to solve a single time step of either the adjoint system or the linearized primal system, where the latter corresponds to computing one Newton step, the solution to a linear problem of the form

$$z^T M_1 x = z^T f \qquad \forall z : M_2 z = 0, \qquad M_2 x = 0 \tag{4.2}$$

has to be calculated. Here, $x = (c_i, w_i, \widetilde{v}_i)$ with $\widetilde{v}_i = v_i - \mathcal{F} u_i$ or $x = (p_i, r_i, q_i)$, respectively. M_1 denotes the system matrix and f the right hand side incorporating values of the state or the adjoint at former times. The matrix M_2 corresponds to the discretization of the mapping $(z_c, z_w, z_v) \mapsto (\int_\Omega z_c, \int_\Omega z_w, \operatorname{div} z_v, z_v|_{\partial\Omega})$, which assembles the mean-value conditions on c, w and p, r, respectively, the incompressibility of v, respectively q, the boundary conditions on $\widetilde{v}$, respectively q, as well as on the corresponding test functions. In order to solve (4.2), note that this problem can be rewritten as a saddle point system, which we solve in exchange

$$\begin{pmatrix} M_1 & M_2^T \\ M_2 & 0 \end{pmatrix} \begin{pmatrix} z \\ \lambda \end{pmatrix} = \begin{pmatrix} f \\ 0 \end{pmatrix}. \tag{4.3}$$

Our implementation uses MATLAB and a direct solver to compute the solution to (4.3). This equation corresponds to solving one time step of the dual system (2.9)–(2.13) or to solving the linearization of the primal system (2.1)–(2.3) in Newton's method. Of course, a suitable preconditioned iterative solver using the Krylov-subspace method could be applied as well to solve (4.3). In order to reduce the computational effort for the direct solver, we use the null space method (see e.g. [24]). For this purpose, note that in two dimensions a spanning system for all divergence-free vector fields $v \in V^{\mathcal{T}}$ is given by the curls of the nodal basis functions joined by the set $v_E \in V^{\mathcal{T}}$ for $E \in \mathcal{E}$ where $v_E(E_m)$ is tangential to E and of unit length, and it satisfies $v_E(E'_m) = 0$ for $E \neq E' \in \mathcal{E}$ (cf. [28]).

5. Numerical results

This section reports on the numerical results which we obtained from our algorithm for solving several test problems including boundary or distributed controls. Here as well as in many applications one is interested in tracking a desired concentration profile c_M^* at final time. Our objective in (2.7), however, includes a desired trajectory, where each L^2-distance to c_i^* is weighted by $\lambda_i \geq 0$. Clearly, for properly chosen $(c_i^*)_{i=0}^M$ and $\lambda_i > 0$ this may help the

control action to reach c_M close to c_M^*. In (2.7) the time instances, where a desired concentration is prescribed, coincide with $(t_i)_{i=0}^M$. Of course, it is conceivable to select desired concentration profiles at different times.

In our numerical tests we select $c_i^* = c_M^*$ for all $i = 0, ..., M-1$ as well as a sequence $((\lambda_i^{(n)})_{i=0}^{M-1})_{n\in\mathbb{N}}$ which decreases in each component as the Yosida parameter α_n tends to 0.

We first present two examples of boundary control and then test cases for distributed control. The ability to steer the phase concentration in the semidiscrete CH-NS system to a desired profile at final time is more challenging (if possible at all) for boundary control when compared to distributed control actions. Topological changes resulting from boundary control, like the splitting of regions of pure phases, seem possible only if the given phase configuration is energetically highly unfavorable. On the other hand, for the distributed control a wide range of target profiles including many relevant ones for applications, are reachable. Examples for such phase patterns can be observed in subsection 5.3 and 5.4 below.

Unless otherwise specified the following parameters are used: As the domain we choose $\Omega = (0,1)^2$ with a uniform triangulation of mesh width $h = 1/128$. We use $T = 0.2$ for the time horizon, and the time interval $[0, T]$ is divided into $M = 30$ subintervals.

The gradient descent method is performed for a fixed number $n_{\max}$ of different Yosida parameters. For the examples of subsections 5.1, 5.2 and 5.4 below we use $n_{\max} = 5$, for the one of subsection 5.3 we use $n_{\max} = 4$. As initial Yosida parameter α_1 we choose $\alpha_1 = 10^{-3}$ for the examples of subsections 5.1, 5.2 and 5.3 and $\alpha_1 = 10^{-2}$ in subsection 5.4. The other values of α_n are given by $\alpha_1(\frac{10^{-6}}{\alpha_1})^{\frac{n-1}{n_{\max}-1}}$ for $n = 2, ..., n_{\max}$. Then $\alpha_{n_{\max}} = 10^{-6}$ and the values of α form a geometric sequence. For the constants entering the semidiscrete CH-NS system we set $Pe = 10$, $K = 2$, $\varepsilon = 6 \cdot 10^{-4}$, and $Re = 200$.

Furthermore, for the extended Armijo line search algorithm (Algorithm 1 in the appendix) we use the parameters $w_c = 1/3$, $w_e = 2$, $z_z = 3$, $z_m = 4$ and $\nu = 10^{-2}$ for boundary control and $\nu = 10^{-3}$ for distributed control, respectively. As criterion for stopping with failure we set $s_{\min} = 10^{-7}$. Finally, we stop our Newton iteration as soon as the residual drops below 10^{-9} in the respective norm. For stopping the gradient descent method we choose the parameters $z_s = 7$, $\theta_n = 10^{-4} \cdot 0.1^{\frac{n-1}{n_{\max}-1}}$ and $\vartheta_n = 10^{-3} \cdot 0.1^{\frac{n-1}{n_{\max}-1}}$ for $n = 1, ..., n_{\max}$. Then $\theta_{n_{\max}} = 10^{-5}$, $\vartheta_{n_{\max}} = 10^{-4}$ and θ and ϑ form geometric

sequences.

5.1. Disk to a ring segment

Our first example of boundary control is the deformation of a disk into a sector of a ring (i.e, we start with a configuration where we have the pure phase $c = 1$ in the given disk and $c = -1$ outside). Figure 1 shows the evolution of the concentration under the applied control, where the initial data containing pure phases only is included in the upper left corner. The desired profile is depicted in the bottom right corner of Figure 1. The action of the control on the boundary is indicated by the vector field on the boundary of the respective box. The length of an arrow indicates the intensity of the control action, and the direction of the control field is given by the orientation of the arrow. Moreover, interfacial regions are displayed in green color.

The aim of this example was the deformation of a stable disk-shaped region into some region which is neither circular nor convex anymore. The figure shows that the algorithm was capable to find a numerical locally optimal control inducing a phase concentration which is rather close to the desired profile. This is apparently achieved by first shifting the disk to the target location and then stretching it by pulling the ends apart (outflow at the lower corners) as well as pushing the middle part upwards due to an inflow from the middle portion of the bottom boundary. Note that the final configuration is unstable, in the sense that the ring segment would again deform into a circular region if the system could evolve naturally, i.e. without a control action.

The following Table 1 provides the iteration numbers for each run with different parameter settings (Yosida parameter and coefficients in the cost functional). It includes the Yosida parameter, the number of gradient steps in the corresponding setting, the average number of line search steps per gradient iterations and the average number of Newton steps used in order to solve the primal system in a single time step.

The results show that the number of line search steps per gradient step is around 2 and that the largest average numbers of Newton steps per time step occurs in the first and the last time step and lies between 6 and 7. The related values of the cost functional are depicted in Figure 2. It can be observed that the graph is piecewise continuous with each piece belonging to one choice of the Yosida parameter. One further observes that each branch is monotonically decreasing over the iterations (horizontal axis). Moreover, the (final)

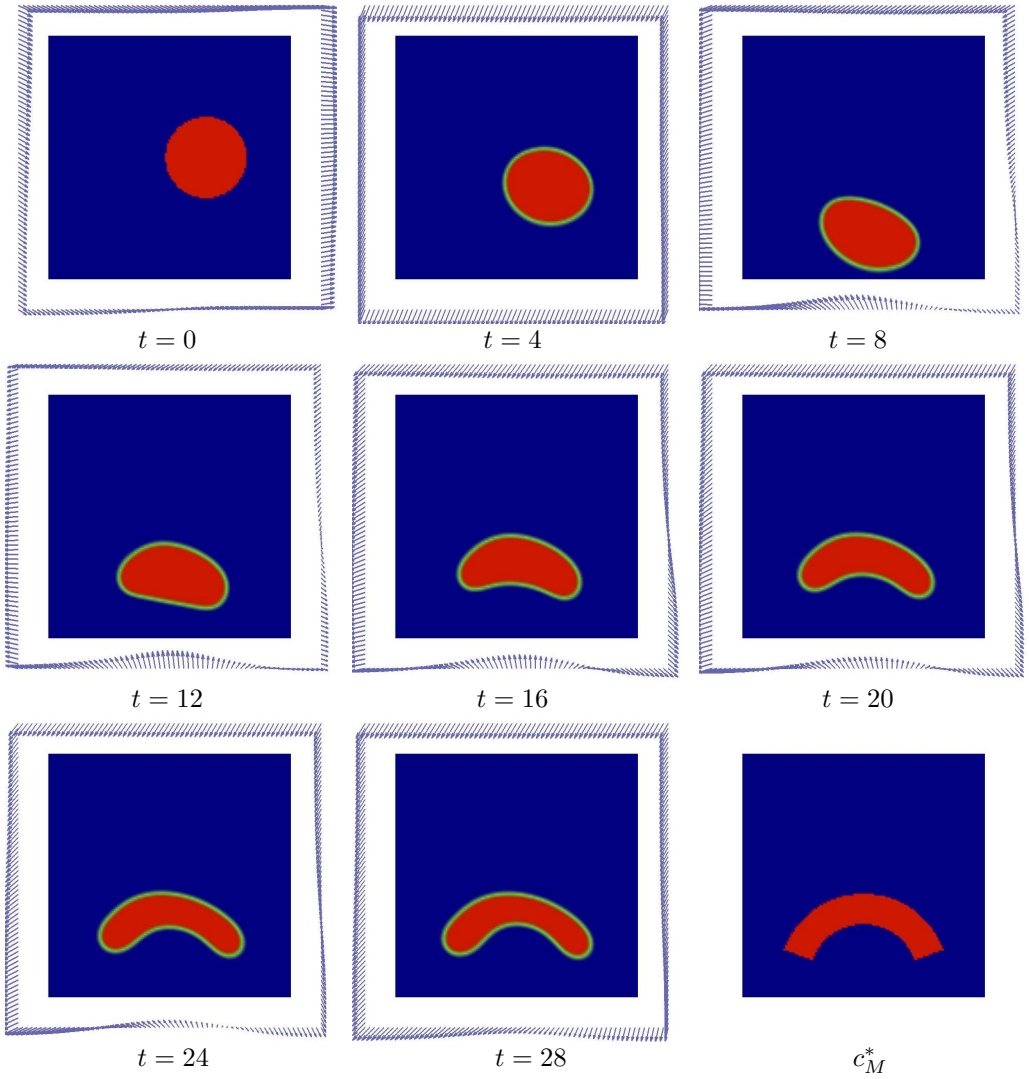

Figure 1: Evolution of the concentration with boundary control to deform a disk into a ring segment (row-wise and from left to right). First and last image are the initial and, respectively, the desired concentrations.

values of the cost functional increase from one branch to the next. This indicates that approximating the original problem and the involved variational inequality makes it more difficult for the control action to steer the system towards the desired state. The rather significant increase of the objective value at the beginning of the branch starting at around iteration 190 can be

Yosida-parameter	grad. steps	line search steps	Newton steps	ø Newton/t
1.00000e-03	119	185	32615	6.08
1.77828e-04	27	56	4964	3.06
3.16228e-05	23	38	3209	2.91
5.62341e-06	14	22	2663	4.17
1.00000e-06	42	85	17320	7.03

Table 1: Iteration numbers for the example "Disk to a ring segment", cf. Figure 1.

attributed to the fact that the numerical solution for the previous α-value does not provide a sufficiently good initial value for the Yosida parameter associated with the branch starting at approximately iteration 190.

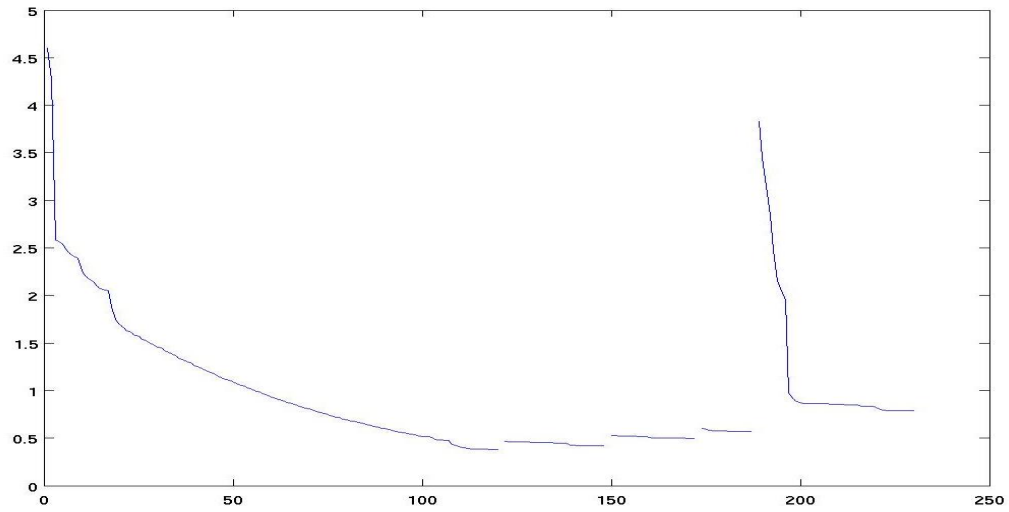

Figure 2: Values of the cost functional after each gradient step (for example 5.1). Each branch corresponds to a specific Yosida parameter α_n.

5.2. Ring to disks

The second example consists of deforming a ring region into four separate disks by using optimal boundary control. The evolution of the phase field and the corresponding control obtained by our algorithm is shown in Figure 3. The control appears to be almost constant in time and with an inflow perpendicular to the boundary at the middle of the faces of Ω and an outflow at the corners. Moreover, the control action drives the concentration

very close to the desired profile, which is depicted in the bottom right plot of Figure 3. The resulting disk-like regions deviate only slightly from the desired shapes and show the expected diffuse interface indicated in green.

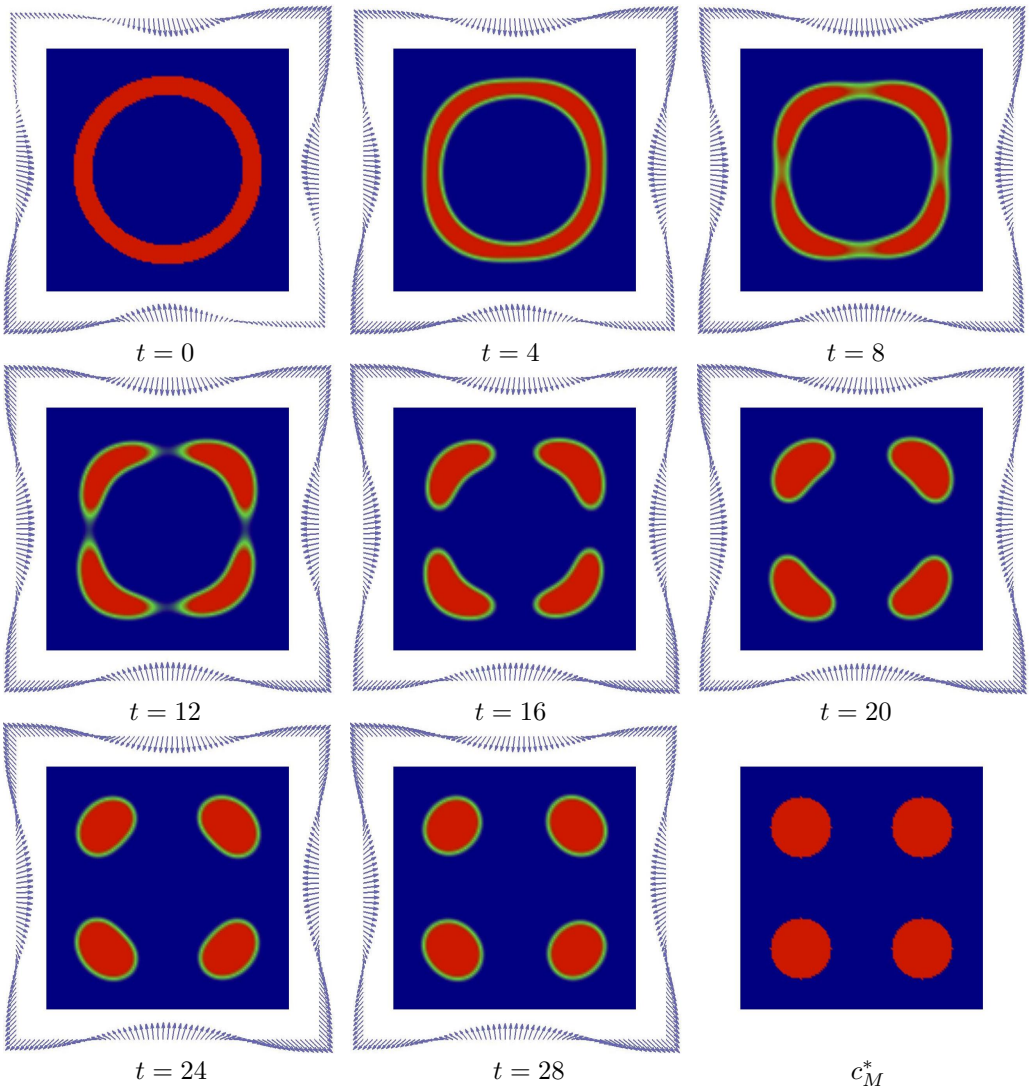

Figure 3: Evolution of the concentration with boundary control in order to transform a ring (first image) into four disks.

Note that the starting configuration possesses a large surface area compared to the area of the region itself and is therefore energetically unfavorable. This instability is the main reason for the success of the control action in this

example. Once initiated by the control, the phase separation process helps in splitting up the ring and drives the evolution forward to the desired disks.

The qualitative behavior of the values of the cost functional is similar to the one in the first test example. The iteration numbers of the algorithm given in Table 2 show that the number of gradient steps decreases with decreasing Yosida parameter. Moreover, the average numbers of Newton iterations for solving the primal systems in the individual time steps, first decrease with decreasing Yosida parameter. But for our smallest choice of the Yosida parameter we notice a significant increase in Newton steps. This behavior can be attributed to the fact that the limit problem is nonsmooth, which causes an increase in curvature of the mollified Yosida approximation, thus reducing the radius for fast local convergence of Newton's method.

Yosida-parameter	grad. steps	line search steps	Newton steps	ø Newton/t
1.00000e-03	18	35	5626	5.54
1.77828e-04	16	34	3810	3.86
3.16228e-05	11	27	2838	3.62
5.62341e-06	9	15	2130	4.90
1.00000e-06	7	13	3788	10.05

Table 2: Iteration numbers for the example "Ring to disks", cf. Figure 3.

5.3. Grid pattern of disks

Our first example involving distributed control concerns the deformation of a disk-shaped region into a grid pattern of smaller disks. The evolution of the concentration (phase field) and the applied control are given in Figure 4. In order to depict the force field given by u in the domain Ω we use a representation where different colors indicate different directions. The correspondence between a color and a direction is shown in Figure 5. Moreover, the modulus (length) of the vector field is encoded in the intensity of the colors where intense colors belong to large moduli and pale colors to small moduli, respectively.

In Figure 4 it can be seen that the control enjoys a rich spatial structure that changes over time and which drives the phase field quite close to the desired state. But since the circular regions of the target profile are very close to each other, the control found by the algorithm is not capable of completely separating the different interfaces from each other and a blending of regions

occurs. Nevertheless, the results of this rather challenging example show the potential of distributed control once the technical realization of the control action can be guaranteed.

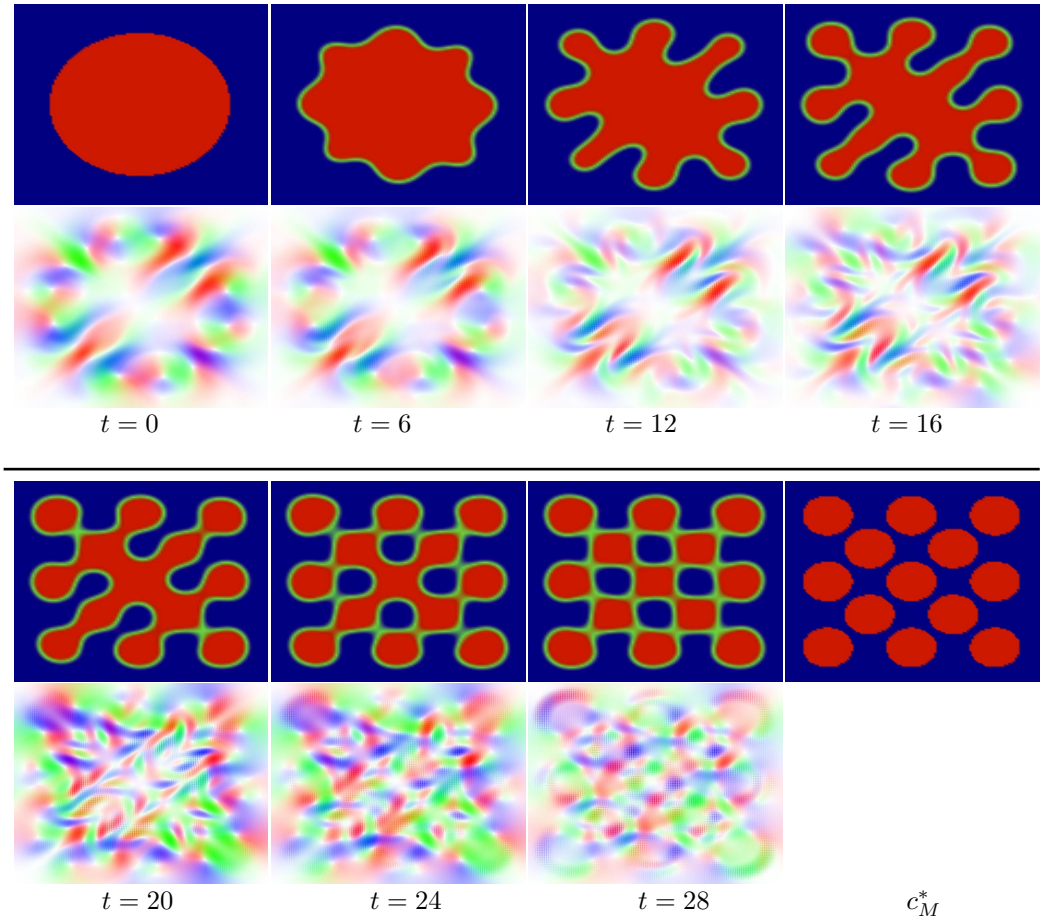

Figure 4: Evolution of the concentration (first and third row) and the corresponding distributed control (second and forth row) to reach a grid of smaller disks from a large disk. The directions of the vector field of the control is represented in a color scheme explained in Figure 5.

Table 3 provides the iteration numbers for this example. Here, the average number of line search steps per gradient step is below 3 and the average number of Newton iterations used in order to solve one time step of the primal system does not exceed 4.4.

The right plot in Figure 5 presents the evolution of the objective values along the iterations. In the branch belonging to the initial Yosida parameter

Yosida-parameter	grad. steps	line search steps	Newton steps	ø Newton/t
1.00000e-03	341	608	77428	4.39
1.00000e-04	39	87	6807	2.70
1.00000e-05	42	104	8670	2.87
1.00000e-06	24	63	6402	3.50

Table 3: Iteration numbers for the example "Grid pattern of disks", cf. Figure 4.

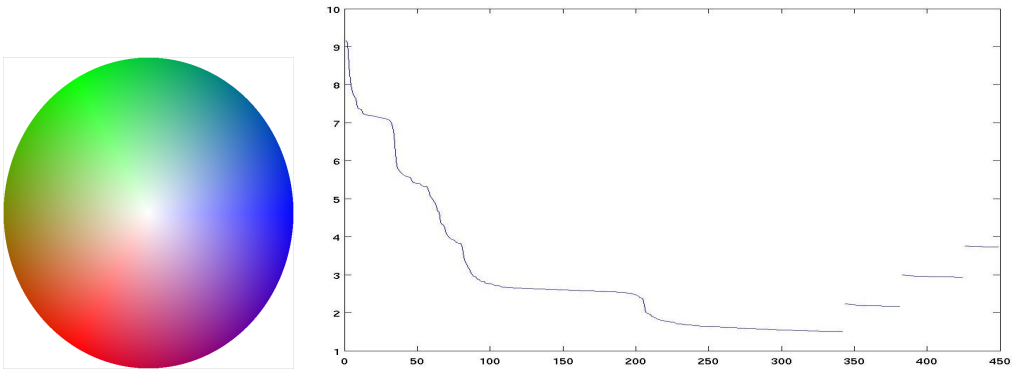

Figure 5: Correspondence between colors and directions (left) and the valued of the cost functional after each gradient step of example 5.3 (right).

a seesaw between iterations with steep descent and iterations with only small descent can be observed. For all of the other parameters the evolution of the cost functional is almost flat indicating that the numerically optimal control found for a large Yosida parameters is numerically almost optimal for smaller parameters as well.

5.4. Grid pattern of finger-like regions

A second example of optimal distributed control of the semidiscrete CH-NS system is shown in Figure 6. Here, the aim is to deform the initial profile of the concentration – again a disk-shaped region – into a pattern of horizontally aligned finger-like regions. The figure shows that the force field given by the control pushes the inner fluid (red) outside along the desired finger pattern. whereas the outer fluid (blue) is pushed vertically to the middle along the desired vacancies between the fingers. This behavior is exactly as one would expect from the optimal control in order to approach the desired profile: distribute both fluids spatially with minimal effort and

then extend the regions occupied by both fluids in those directions that match the desired profile.

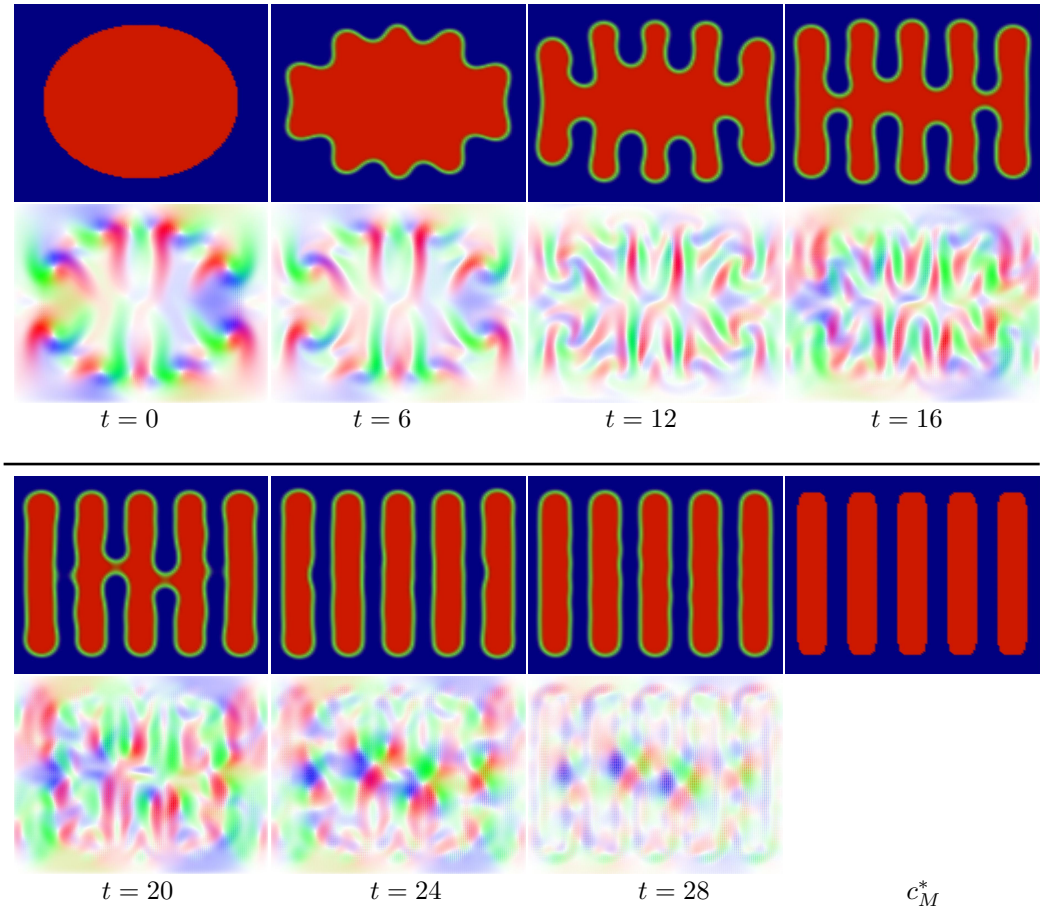

Figure 6: Evolution of the concentration (first and third row) and the corresponding distributed control (second and forth row) to obtain finger-like regions out a disk.

In this example and apart from the inevitable formation of an interfacial region the final concentration almost perfectly fits the desired profile. Since the finger-like regions of the given target are sufficiently separated from each other blending of interfacial regions, as it occurred in the previous example, does not occur.

Table 4 provides the information on the iterations for this example.

Yosida-parameter	grad. steps	line searches	Newton steps	ø Newton/t
1.00000e-02	701	961	158925	5.70
1.00000e-03	19	27	3235	4.13
1.00000e-04	53	110	9829	3.08
1.00000e-05	20	36	3565	3.41
1.00000e-06	11	16	2841	6.12

Table 4: Iteration numbers for the example "Grid pattern of finger-like regions", cf. Figure 6.

6. Conclusions

This paper presented optimal control problems for a time discretized two-phase flow model. The governing state equations consisted of a coupled Cahn–Hilliard/Navier–Stokes system and we considered boundary as well as distributed control of the Navier–Stokes part. First order optimality conditions were given. An algorithmic scheme was presented which is based on a sequence of Yosida-type approximations of the original problem linked via a path-following method. Upon spatial discretization the individual Yosida regularized problems were solved using a gradient descent method and an extended Armijo line search. We concluded our discussion with reports on the behavior of our algorithm for several numerical test cases.

Acknowledgments

The authors gratefully acknowledge support by DFG Research Center MATHEON under project C28 "Optimal control of phase separation phenomena" and by DFG SPP 1506 "Transport Processes at Fluidic Interfaces". M.H. further acknowledges support through FWF under START-program Y305-N18 "Interfaces and Free Boundaries".

Algorithm 1: Armijo line search with expansion

Input: $d^{(n,k)}(= -J^{-1}\hat{\mathcal{J}}'(u^{(n,k)}))$, $s^{(n,k-1)}$, $z \in \mathbb{N}$.

Parameters: $\nu \in (0,1)$, $w_c \in (0,1)$, $w_e > 1$, $z_z, z_m \in \mathbb{N}$, $s_{\min} > 0$.

step 0. Set $s^{(n,k,l)} := s^{(n,k-1)}$, $z^{(l)} := z$, $z_e := 0$.

step 1. **If** $\hat{\mathcal{J}}(u^{(n,k)} + s^{(n,k,l)}d^{(n,k)}) \leq \hat{\mathcal{J}}(u^{(n,k)}) + \nu s^{(n,k,l)}\langle \hat{\mathcal{J}}'(u^{(n,k)}), d^{(n,k)}\rangle$, **then**
  if $z_e = 0$ **then** continue with step 2.
  else continue with step 5.
  end
else
  if $z_e = 0$ **then** continue with step 3.
  else continue with step 6.
  end
end

step 2. Set $z^{(l)} := z^{(l)} + 1$.
if $z^{(l)} \geq z_z$ **then** continue with step 4.
else
  stop with $s^{(n,k)} := s^{(n,k,l)}$, $z := z^{(l)}$
end

step 3. Set $s^{(n,k,l+1)} := w_c s^{(n,k,l)}$, $l := l + 1$, $z^{(l)} := 0$.
if $s^{(n,k,l)} < s_{min}$ **then** stop with failure,
else return to step 1.
end

step 4. Set $s^{(n,k,l+1)} := w_e s^{(n,k,l)}$, $l := l + 1$, $z^{(l)} := 0$, $z_e := z_e + 1$ and return to step 1.

step 5. **If** $z_e < z_m$ **then** return to step 4
else
  stop with $s^{(n,k)} := s^{(n,k,l)}$, $z := z^{(l)}$
end

step 6. Stop with $s^{(n,k)} := w_a^{-1} s^{(n,k,l)}$, $z := z^{(l)}$.

References

[1] S. Aland, S. Boden, A. Hahn, F. Klingbeil, M. Weismann, and S. Weller. Quantitative comparison of Taylor flow simulations based on sharp-

interface and diffuse-interface models. *International Journal for Numerical Methods in Fluids*, 73(4):344–361, 2013.

[2] S. Aland, J. Lowengrub, and A. Voigt. Particles at fluid-fluid interfaces: A new Navier-Stokes-Cahn-Hilliard surface-phase-field-crystal model. *Phys. Rev. E*, 86:046321, 2012.

[3] S. Aland, S. Schwarz, J. Fröhlich, and A. Voigt. Modeling and numerical approximations for bubbles in liquid metal. *The European Physical Journal Special Topics*, 220(1):185–194, 2013.

[4] S. Aland and A. Voigt. Benchmark computations of diffuse interface models for two-dimensional bubble dynamics. *International Journal for Numerical Methods in Fluids*, 69(3):747–761, 2012.

[5] S. Aland and A. Voigt. Simulation of common features and differences of surfactant-based and solid-stabilized emulsions. *Colloids and Surfaces A: Physicochemical and Engineering Aspects*, 413(0):298–302, 2012.

[6] V. Barbu. *Nonlinear Semigroups and Differential Equations in Banach Spaces*. Editura Academiei Republicii Socialiste România, Bucharest, 1976.

[7] V. Barbu. *Optimal Control of Variational Inequalities*, volume 100 of *Research Notes in Mathematics*. Pitman (Advanced Publishing Program), Boston, MA, 1984.

[8] J.F. Bonnans, J.C. Gilbert, C. Lemaréchal, and C.A. Sagastizábal. *Numerical Optimization. Theoretical and Practical Aspects. Transl. from the French.* Universitext. Berlin: Springer., 2003.

[9] J.W. Cahn and J.E. Hilliard. Free energy of a nonuniform system. I. Interfacial free energy. *J Chem. Phys.*, (2):258–266, 1958.

[10] H. Choi, M. Hinze, and K. Kunisch. Instantaneous control of backward-facing step flows. *Appl. Numer. Math.*, 31(2):133–158, 1999.

[11] M. Crouzeix and P.-A. Raviart. Conforming and nonconforming finite element methods for solving the stationary Stokes equations. I. 1974.

[12] S. Eckert, P. Nikrityuk, B. Willers, D. Räbiger, N. Shevchenko, H. Neumann-Heyme, V. Travnikov, S. Odenbach, A. Voigt, and K. Eckert. Electromagnetic melt flow control during solidification of metallic alloys. *The European Physical Journal Special Topics*, 220(1):123–137, 2013.

[13] A. Ern and J.-L. Guermond. *Theory and Practice of Finite Elements.* Applied Mathematical Sciences 159. New York, Springer., 2004.

[14] H. Farshbaf-Shaker. A penalty approach to optimal control of Allen-Cahn variational inequalities: MPEC-view. Preprint 06, Department of Mathematics, University of Regensburg, Germany, 2011.

[15] R. Glowinski and A.M. Ramos. A numerical approach to the Neumann control of the Cahn-Hilliard equation. In *Computational Methods for Control and Applications. Gakuto International Series: Mathematical Sciences and Applications, Vol. 16*, pages 111–155, Tokyo, 2002. Gakkotosho Co.

[16] M. Hintermüller, M. Hinze, and C. Kahle. An adaptive finite element Moreau-Yosida-based solver for a coupled Cahn-Hilliard/Navier-Stokes system. *Journal of Computational Physics*, 235(0):810–827, 2013.

[17] M. Hintermüller and D. Wegner. Distributed optimal control of the Cahn-Hilliard system including the case of a double-obstacle homogeneous free energy density. *SIAM J. Control Optim.*, 2013.

[18] M. Hintermüller and D. Wegner. Optimal control of a semidiscrete Cahn-Hilliard-Navier-Stokes system. *SIAM J. Control Optim.*, 52(1):747–772, 2014.

[19] M. Hinze and C. Kahle. A nonlinear model predictive concept for control of two-phase flows governed by the Cahn-Hilliard Navier-Stokes system. Hömberg, Dietmar (ed.) et al., System modeling and optimization. 25th IFIP TC 7 conference on system modeling and optimization, Berlin, Germany, September 12–16, 2011. IFIP Advances in Information and Communication Technology 391, 348-357 (2013), 2013.

[20] P. C. Hohenberg and B. I. Halperin. Theory of dynamic critical phenomena. *Rev. Mod. Phys.*, 49:435–479, 1977.

[21] K. Ito and K. Kunisch. Receding horizon optimal control for infinite dimensional systems. *ESAIM, Control Optim. Calc. Var.*, 8:741–760, 2002.

[22] J. Kim, K. Kang, and J. Lowengrub. Conservative multigrid methods for Cahn-Hilliard fluids. *Journal of Computational Physics*, 193(2):511–543, 2004.

[23] J. Kim and J. Lowengrub. Interfaces and multicomponent fluids. In J-P. Franoise, G.L. Naber, and T.S. Tsun, editors, *Encyclopedia of Mathematical Physics*, pages 135 – 144. Academic Press, Oxford, 2006.

[24] J. Nocedal and S.J. Wright. *Numerical optimization. 2nd ed.* Springer Series in Operations Research and Financial Engineering. New York, NY: Springer., 2006.

[25] Y. Oono and S. Puri. Study of phase-separation dynamics by use of cell dynamical systems. I. Modeling. *Phys. Rev. A*, 38(1):434–453, 1988.

[26] S. Praetorius and A. Voigt. A phase field crystal model for colloidal suspensions with hydrodynamic interactions. arXiv:1310.5495, 2013.

[27] W. Rudin. *Functional Analysis. 2nd ed.* McGraw-Hill, New York., 1991.

[28] I.A. Segal. Finite element methods for the incomressible Navier-Stokes equations. Delft University of Technology, 2012.

[29] Q.-F. Wang and S. Nakagiri. Weak solutions of Cahn-Hilliard equations having forcing terms and optimal control problems. *Research Institute for Mathematical Sciences, Kokyuroku*, 1128:172–180, 2000.

[30] J. Yong and S. Zheng. Feedback stabilization and optimal control for the Cahn-Hilliard equation. *Nonlin. Analysis. Theory, Meth. & Appls.*, 17(5):431–444, 1991.

[31] X. Zhao and C. Liu. Optimal control problem for viscous Cahn-Hilliard equation. *Nonlinear Anal., Theory Methods Appl., Ser. A, Theory Methods*, 74(17):6348–6357, 2011.

[32] X. Zhao and C. Liu. Optimal control of the convective Cahn-Hilliard equation. *Appl. Anal.*, 92(5):1028–1045, 2013.

[33] B. Zhou, Massachusetts Institute of Technology. Dept. of Materials Science, and Engineering. *Simulations of Polymeric Membrane Formation in 2D and 3D*. Massachusetts Institute of Technology, Dept. of Materials Science and Engineering, 2006.

[34] J. Zowe and S. Kurcyusz. Regularity and stability for the mathematical programming problem in Banach spaces. *Appl. Math. Optimization*, 5:49–62, 1979.